Chapter 16

Numerical Study of Turbulent Flows and Heat Transfer in Coupled Industrial-Scale Tundish of a Continuous Casting Material in Steel Production

Jose Adilson de Castro, Bruno Amaral Pereira,
Roan Sampaio de Souza,
Elizabeth Mendes de Oliveira and
Ivaldo Leão Ferreira

Additional information is available at the end of the chapter

http://dx.doi.org/10.5772/intechopen.75935

Abstract

This chapter describes the numerical simulations of a coupled industrial scale of the tundish and continuous casting process. The governing equations are presented, and the numerical procedure is discussed in a common framework. The coupled solutions are presented for the transient turbulent flows within the tundish, solidifying zone and extracting regions with the coupling phenomena of heat and mass transfer. The tundish region flow and refractory are calculated using the inlet and outlet boundary conditions in order to estimate the filling phenomena. The transitions and cooling zones for the thin slab continuous casting process are designed to account for the control of the solidified skin in order to avoid breakout. We compared the numerical predictions of the temperatures with industrial monitoring data for a reference case in order to verify the consistence of the model predictions. A parallel version of the numerical code is proposed aiming to improve the computation time keeping numerical accuracy.

Keywords: tundish, continuous casting, turbulent flow, numerical modelling, thin slab, finite volume

1. Introduction

The steel production in an integrated mill requires complex operation units and demands a large amount of energy. In the operation units comprising the transformation of the liquid steel

into slabs, several aspects of the product quality are assured [1–6]. The security and stability of the operations as well as the productivity with lower defects are the main concern and have driven the new development on this step. Of special interest is to fit the dimensions of the slabs suitable for further hot working processes free of internal and superficial defects. The strict control of these steps is the primary effort to high-quality steel slab. A general schematic overview of the continuous casting facilities including the metal transfer steps is presented in **Figure 1**. The initial step is the metal transfer from the ladle to the tundish filling the vessel and establishing the synchronised mass flows. The tundish distributor is used to control the feeding rate of the oscillating mould of the continuous casting step using the submerse tune and flowing valve control. The heat transfer and the flowing phenomena within the oscillating mould are key phenomena to attain the adequate microstructure of the solidified steel and keep the safety of the process with the formation of the solidification skin, which plays the major role on the cooling zones for final solidification of centre of the slab.

The synchronised control of the cooling rate along the mould, bender, speed, and radiation regions is the key for a successful operation of the entire system. In order to improve the process safety, control and productivity comprehensive mathematical models have been developed separately for the tundish and continuous casting processes [1, 4]. Progress in computational simulation has provided tools to help to comprehend the processes. Consequently, several investigations of the parameters which affect the performance under safety operation conditions were driven [3–7]. The tundish operation is carried out in order to assure the compositional and thermal homogeneity of the liquid with low level of impurities and inclusions. The caster machine is designed to promote continuous solidification of liquid metal fed by a tundish through a submerse valve. In the mould region, a strong heat flux is imposed, and a thick solid shell is formed. Water cooling is continuously applied until a secondary region is

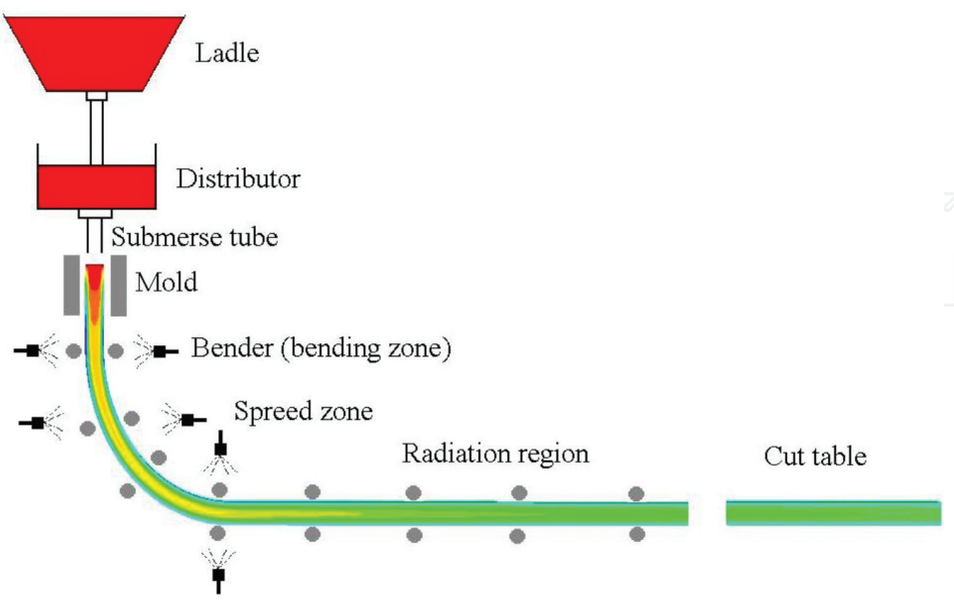

Figure 1. Schematic view of coupling of ladle feeding, tundish and continuous casting process and facilities.

http://dx.doi.org/10.5772/intechopen.75935

reached, where the cooling is performed only by radiation. At the end of the vein, the slab is cut and discharged on a rolled table. Due to process complexity, which involves heat transfer coupled with phase transformation and fluid flow, the prediction of process parameters and their optimization is usually performed by using empirical procedures. However, the development of efficient numerical techniques and the availability of fast and low-cost computers has bust recently the simulation of real operational conditions [8–13]. To date, it is possible to investigate virtually the manufacturing of several kinds of steels aiming low cost and high material efficiency. Several works in the literature have been reported to analyse the metal behaviour within the oscillating mould of the caster machine due to its importance on the productivity and on the product final quality [4–15]. The oscillating mould is an important component of the caster machine and has strong influence on surface defects and on the temperature distribution inside the mould [2–8]. The heat transfer analysis during solidification is traditionally performed by analytical and numerical methods. Although analytical methods are more elegant, they require a series of assumptions that usually lead to a considerable simplification of the physical phenomena producing unrealistic or limited solutions. Considering numerical methods, four techniques are commonly used: finite differences [7–11], finite elements [12–15], finite volumes [16] and boundary elements [17]. These methods are able to solve the energy, the mass, species and momentum equations. In order to improve scientific calculation performance, continuous changes have been arisen in computational platform paradigm. In the past, the scientific simulation was normally performed in shared memory large computers or in common sequential computers [18]. The fast rate of development in processor technology and the commercial availability of inexpensive powerful personal computers have created a perfect scenario to build up cluster of personal computers as an alternative to the larger and more expensive ones [19]. As consequence of low price, easy maintenance and powerful processors, these so-called Beowulf clusters are becoming popular among scientific computational groups. This architecture offers collective memory to solve scientific complex problems [17, 21]. Although the rise of distributed computer platforms was only an alternative for high-cost supercomputer solutions, they changed profoundly the rule of code development, which now needs to encompass distributed machines [18, 19]. Distributed platforms are suitable for problems in which domain can be split up into small subdomains containing common boundaries. Most CFD codes demand high amount of memory, which is normally available in distributed memory architecture [17, 18]. However, for accuracy and consistency reasons, a parallel implementation needs to interchange information with subdomain boundaries. This synchronisation scheme leads to an increase in the data transfer time due to the existence of a synchronisation elapsed time [17–21]. The communication among computers is carried out by using libraries of Message Passing Interface (MPI) [25]. The library Message Passing Interface (MPI) has largely been used in its freeware version called MPICH [17–21]. In this context, this work newly presents a multidomain parallel numerical model able to simulate the continuous casting of steel. The main objective is to demonstrate the validity of the model and point out the improvement in calculation speedup by developing a code based on multidomain parallel MPI compared to a serial and to a simple MPI parallel code. All the computer codes used in this study are homemade ones, which were developed and tested by the authors.

2. A unified formulation for the tundish and continuous casting processes

The tundish and continuous casting operation units are connected by metal transfer systems to account for the smooth operation and strict control of both. However, a common formulation is possible based on transport phenomena principles. In this section we present a turbulent flow coupled with heat and mass transfer for interconnected processes. The tundish is modelled as a reactor including the metal, slag and inclusions flows, while the refractories and internal protective devices are considered. A multiphase formulation is considered: (a) liquid metal, (b) liquid slag, (c) solidified metal, (d) solidified slag, (e) particle inclusions and (f) refractory:

$$\frac{\partial(\rho u_i)}{\partial t}+\frac{\partial}{\partial x_j}\left(\rho u_j u_i\right)=\frac{\partial}{\partial x_j}\left(\left(\mu+\mu_t\right)\frac{\partial u_i}{\partial x_j}\right)-\frac{\partial}{\partial x_j}\left(\tau_{ij}+C_{ij}+L_{ij}\right)-\frac{\partial P}{\partial x_i}-\frac{\left(1-f_s\right)}{K_{u_i}}u_i+\rho g_{ui} \tag{1}$$

$$\frac{\partial(\rho T)}{\partial t}+\frac{\partial}{\partial x_j}\left(\rho u_j T\right)=\frac{\partial}{\partial x_j}\left(\left(\frac{k}{Cp}+\frac{k_t}{Cp_t}\right)\frac{\partial T}{\partial x_j}\right)-\frac{\partial}{\partial x_j}\left(\theta+C+L\right)-\frac{\partial}{\partial t}\left(\rho\Delta H f_s\right) \tag{2}$$

$$\frac{\partial(\rho)}{\partial t}+\frac{\partial}{\partial x_j}\left(\rho u_j\right)=0 \tag{3}$$

$$\frac{\partial}{\partial t}\left(\rho C^i\right)\ +\ \frac{\partial\left(\rho u_j C^i\right)}{\partial x_j}=\frac{\partial}{\partial x_j}\left(\left(D^i+\frac{\mu_t}{\rho}\right)\frac{\partial\left(C^i\right)}{\partial x_j}\right) \tag{4}$$

$$\frac{\partial(\rho k)}{\partial t}+\frac{\partial}{\partial x_j}\left(\rho u_j k\right)=\frac{\partial}{\partial x_j}\left(\left(\mu+\frac{\mu_t}{\sigma_k}\right)\frac{\partial k}{\partial x_j}\right)+2\mu_t S_{ij}S_{ij}-\rho\varepsilon+\beta g_i\frac{\mu_t}{\mathrm{Pr}}\frac{\partial T}{\partial x_i} \tag{5}$$

$$\frac{\partial(\rho\varepsilon)}{\partial t}+\frac{\partial}{\partial x_j}\left(\rho u_j\varepsilon\right)=\frac{\partial}{\partial x_j}\left(\left(\mu+\frac{\mu_t}{\sigma_e}\right)\frac{\partial\varepsilon}{\partial x_j}\right)+C_{1e}\frac{\varepsilon}{k}\left(2\mu_t S_{ij}S_{ij}+C_{3e}\beta g_i\frac{\mu_t}{\mathrm{Pr}}\frac{\partial T}{\partial x_i}\right)-C_{2e}\rho\frac{\varepsilon^2}{k} \tag{6}$$

where g_u is the gravity acceleration component at the velocity component direction, depending on the number of species, which can be written as

$$g_u={}^{u}g_0\sum_{C,\,Mn}\left[\beta_S^i\left(C_l^i-C_{l,0}^i\right)+\beta_T^i(T-T_0)\right] \tag{7}$$

Viscosity was treated as effective viscosity [21] in the following form:

$$\mu_{eff}=\frac{\overline{\sigma}}{3\overline{\varepsilon}}+\mu_t \tag{8}$$

$$\mu_t=(\Delta)^2\sqrt{S_{ij}S_{ij}} \tag{9}$$

where $\overline{\sigma}$ is the material mean stress and $\overline{\varepsilon}$ is the effective deformation rate presented by Zienkiewicz [22] and Δ is a sub-grid scale for the isotropic turbulence filtering. All the variables used in the formulation are taken as the filtered values. The constants $c_{1\varepsilon}=1.44$, $c_{2\varepsilon}=1.92$, $c_{3\varepsilon}=0.09$ and $\sigma_\varepsilon=1.30$ are related with turbulent kinetic energy (k) and its dissipation rate (ε):

http://dx.doi.org/10.5772/intechopen.75935

$$\tau_{ij} = \mu_t \left(\frac{\partial u_i}{\partial x_j} + \frac{\partial u_j}{\partial x_i} \right) + \frac{2}{3} k \delta_{ij} \tag{10}$$

$$L_{ij} + C_{ij} = \frac{\Delta_k}{12} \left(\frac{\partial u_i}{\partial x_k} + \frac{\partial u_j}{\partial x_k} \right) \tag{11}$$

$$S_{ij} = \frac{1}{2} \left(\frac{\partial u_i}{\partial x_j} + \frac{\partial u_j}{\partial x_i} \right) \tag{12}$$

In the solid phase, thermal conductivity was assumed as a function of temperature, according in Holman [23]:

$$k = \psi - 0.01 \gamma T \tag{13}$$

where ψ and γ are constants for a specific metal alloy and the refractories considered for each layer and formed solidified shell. For the liquid phases, a similar relationship is assumed with their specific constants.

The specific heat for the solid and the liquid phases is obtained directly from ThermoCalc calculation using TCFE5 database, while for the refractories, specific relations are used depending on the materials used [24].

The local liquid concentration of each species is given by

$$\left[C_l^C\right]_P = \frac{[\rho C]_P^C - [\rho C]_P^{C,\,old} + \left[\rho_l g_P^{old} + \beta^C \rho_S \left(1 - g_P^{old}\right) k_0^C\right] \left[C_l^C\right]_P^{old}}{\rho_l g_P^{n+1} + \beta^C \rho_S \left(1 - g_P^{n+1}\right) k_0^C + \left(1 - \beta^C\right) \rho_S k_0^C \left(g_P^{old} - g_P^{n+1}\right)} \tag{14}$$

$$\left[C_l^{Mn}\right]_P = \frac{[\rho C]_P^{Mn} - [\rho C]_P^{Mn,\,old} + \left[\rho_l g_P^{old} + \beta^{Mn} \rho_S \left(1 - g_P^{old}\right) k_0^{Mn}\right] \left[C_l^{Mn}\right]_P^{old}}{\rho_l g_P^{n+1} + \beta^{Mn} \rho_S \left(1 - g_P^{n+1}\right) k_0^{Mn} + \left(1 - \beta^{Mn}\right) \rho_S k_0^{Mn} \left(g_P^{old} - g_P^{n+1}\right)} \tag{15}$$

The segregation parameter β can vary as $0 \leq \beta \leq 1$. Assuming β=1 means the lever rule, and β=0, provides Scheil's equation [24].

The heat flux boundary conditions for the continuous caster machine are estimated depending on the region and operational conditions. In the mould and in the foot roll, the cooling water flow is specified at the four faces, internal and external large faces and right and left narrow faces, while at the other zones, heat fluxes were imposed only at two faces, the internal and the external large faces. For both processes the initial conditions are specified by the measured operational conditions or temperature monitoring data.

Heat fluxes on the water-cooled surfaces and on the radiation zones are given by

$$k \frac{\partial T}{\partial x} = h_{eff} \left(T_{sur} - T_e \right) + \sigma_r \varepsilon_r \left(T_{sur}^4 - T_e^4 \right) \tag{16}$$

where h_{eff} is the effective heat transfer coefficient provided by Eq. (17), T_{sur} is the surface temperature, T_e is the environment temperature, σ_r is the Stefan-Boltzmann constant and ε_r is the emissivity.

The heat transfer coefficient in the sprays zones (foot roll, bender and secondary cooling zone) was obtained by the water cooling enthalpy balance, providing

$$h_{eff} = \frac{m_w c_p \Delta T}{A(T_{sur} - T_e)} \tag{17}$$

where m_w is the water flow, c_p is the water-specific heat, A is the cross-sectional area and ΔT is the water temperature difference given as a setup parameter for the cooling system.

The mould region was modelled by using the steel residence time in the mould to calculate the effective heat transfer coefficient. This coefficient regards the effect of thermal resistance due to air gap formation:

$$h_{mold} = 1004.6 \exp(0.02\, t_m) \tag{18}$$

where t_m is the steel residence time, calculated by means of the cast velocity setup (V_c) and the mould height (Y) as

$$t_m = \frac{Y}{V_c} \tag{19}$$

The inlet and outlet boundary conditions are specified using mass flow, compositions and temperatures. The wall standard log law is used for modelling the liquid to walls and barrier interfaces in both domains of the tundish and continuous casting vein. **Figure 2** shows the geometry and computational domain of the tundish with the refractories and internal barriers. The numerical mesh used was obtained by using continuous refinement using 20% of the total volume increment of each calculation for a standard operational conditions assuming averaged error less than 1% on the temperature and velocity fields. Same procedure was used to obtain the suitable mesh distribution along the continuous casting vein. The final mesh total volumes in the tundish domain were 201,300 and for the continuous casting vein were 288,000.

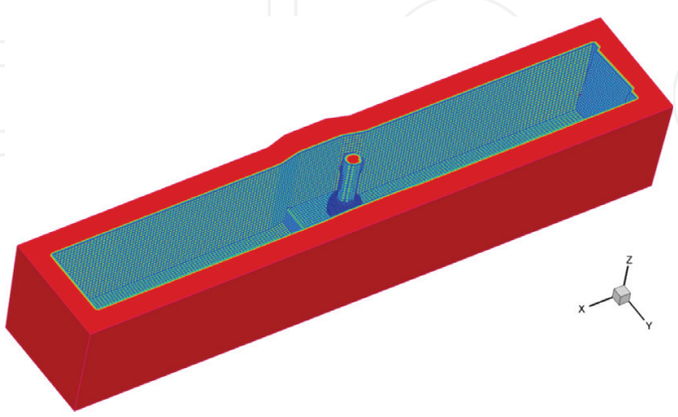

Figure 2. Physical and computational domains including the refractory layers and internal features of the tundish (60 ton).

http://dx.doi.org/10.5772/intechopen.75935

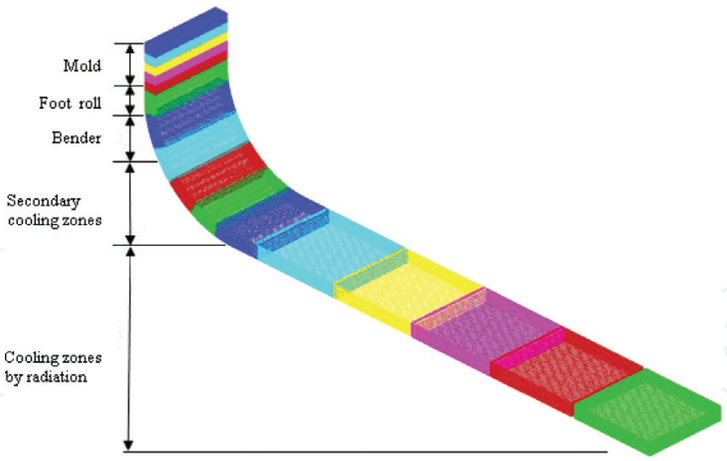

Figure 3. Physical and computational domains indicating the zones of the continuous casting slab and subdomains.

One additional restriction for the continuous casting vein was imposed by using 20% of the total volumes on the oscillating mould region to account for the accuracy of the solution in this region due to the strong gradients developed within the oscillating mould with solidifying shell with strong heat release and solute redistribution. Details of the mesh generated and the subdomains assumed in the simulations are presented in **Figure 3**.

The turbulent quantities at the inlet and outlet are calculated based on the averaged velocities for both processes, as follows:

$$U_{av} = \frac{Q}{A} \tag{20}$$

$$k_{av} = 0.01(U_{av})^2 \tag{21}$$

$$\varepsilon_{av} = \frac{2}{D}(k_{av})^{2/3} \tag{22}$$

Eqs. (20)–(22) are applied depending on the geometry of the valves and feeding systems. The averaged values for the temperature and compositions are either set using the measured values or, in the case of transfer system, the values calculated in the previous connected domains.

The thermophysical properties of the liquids (steel and slags) and solids formed during the solidification process are determined by using computational thermodynamics database. The solid barriers such as refractories and inhibitors are included by using their tabled thermophysical property data furnished by the suppliers. By using the thermodynamics database, a typical steel is modelled using their pseudo-binary diagrams. **Figure 4** shows the temperatures and phase composition dependency for the whole system and specific regions of the diagram. These data are continuously accessed for local predictions of the thermophysical properties during the transient calculation.

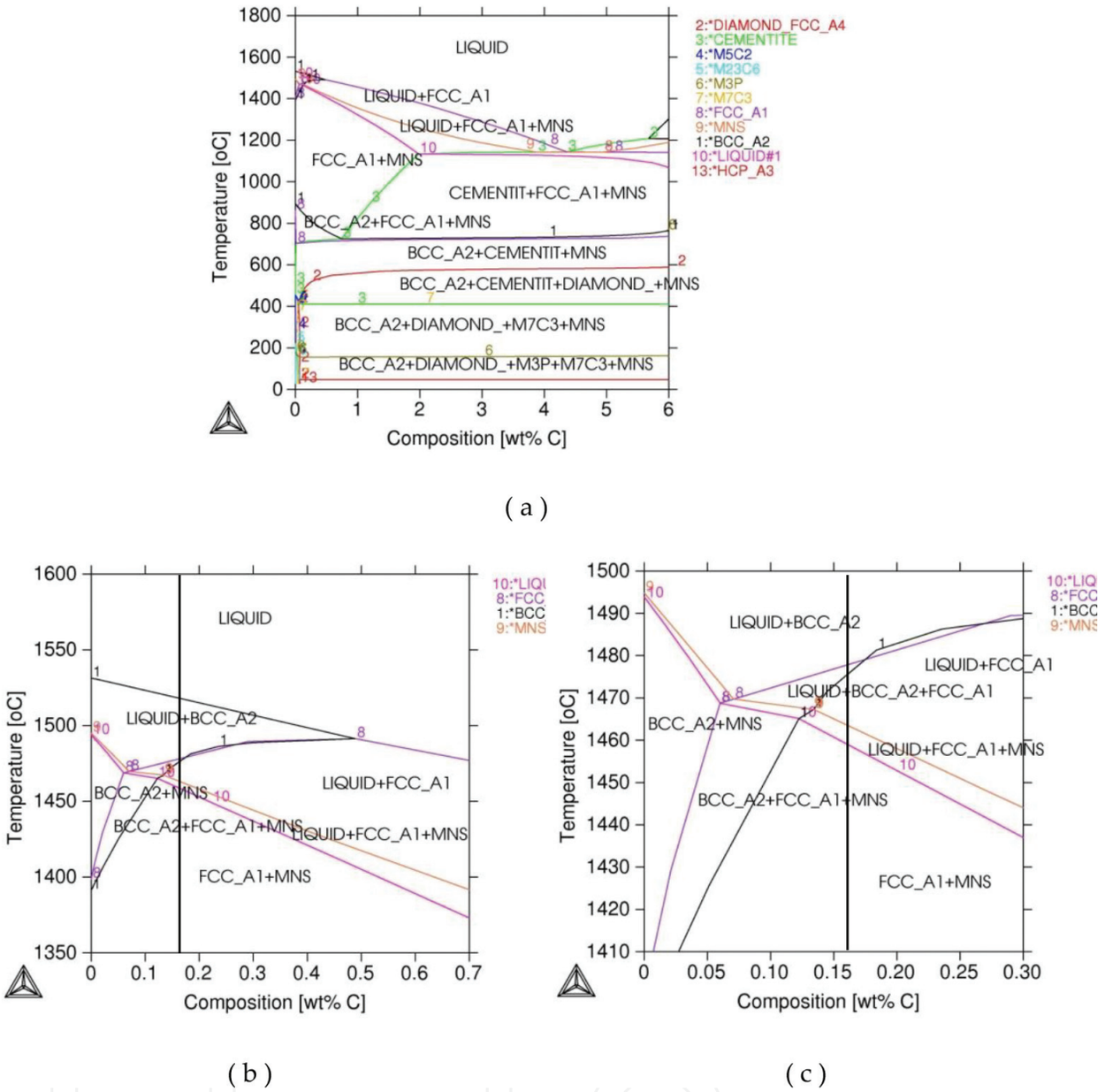

Figure 4. Pseudo-binary phase diagram of Fe-C-Mn-P-S as a function of carbon content (a) phase diagram, (b) and (c) magnification of high temperature range closed to 0, 15 wt% C, which is close to the steel used in this study.

Figure 5 shows the density and heat of phase transformation during temperature evolution. These quantities are accessed to estimate the heat capacity and latent heat released during the solidification and flowing paths. **Figure 6** shows the solid fraction during the solidification path considering the local conditions predicted by computational thermodynamics. With these parameters and physical properties, all the information need for the coupled calculation of the tundish and continuous casting operation are closed.

http://dx.doi.org/10.5772/intechopen.75935

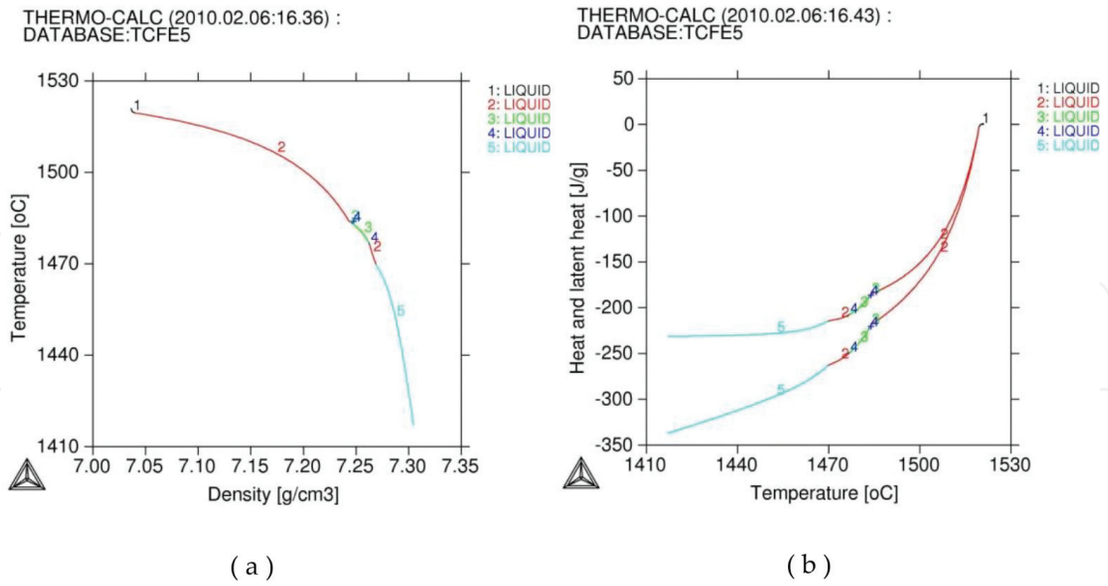

(a) (b)

Figure 5. Thermophysical properties inside mushy zone: (a) density and (b) heat and latent heat for the steel used in this computational modelling.

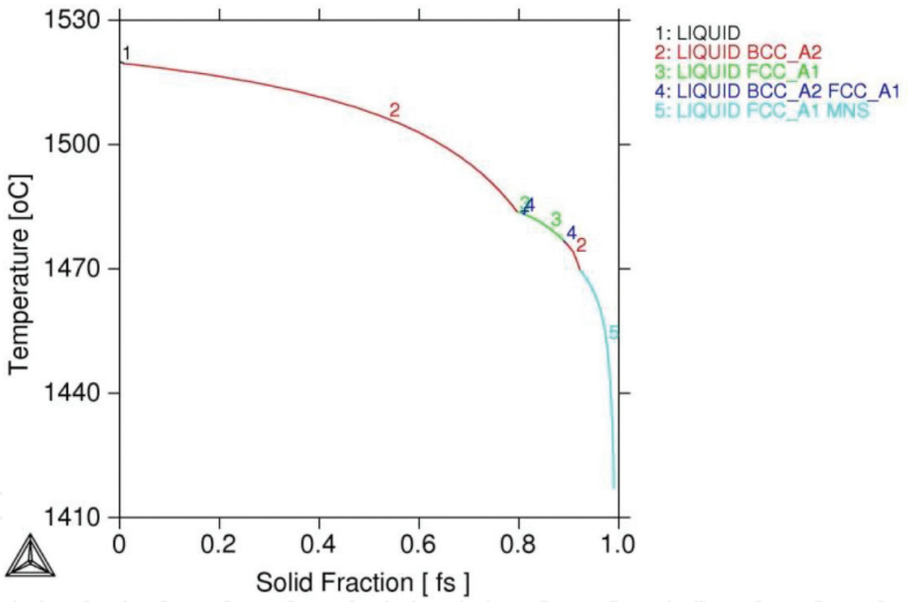

Figure 6. Solid fraction of all solids as a function of temperature during the solidification process within the steel slab used during the calculations accessed from the thermodynamic database.

3. Numerical features

Momentum, mass, energy and species equations were discretizated by using the finite volume method (FVM) applied for general coordinate system [25, 26], where the integration is taken

over a typical control volume. The final product of this operation is a set of algebraic equations. Coefficients are obtained by the so-called power law scheme, according to Patankar [26]. The SIMPLE algorithm is used to iteratively determine the velocity components and pressure linked equations. The numerical solution of the set of algebraic equations demands large computational effort. A line-by-line solver based on the tridiagonal matrix algorithm (TDMA) was used to solve the system of algebraic equations. The Alternate Direction Implicit (ADI) iterative procedure was applied within a common solver for all discretized equations. The iterative solution was obtained for each time step in a fully implicit scheme [25, 26]. The convergence criteria were used for all variables admitting a maximum local error less than 1% for all variables simultaneously.

4. Analysis cases

In order to show the capability of the coupled model, a sequence of tundish filling and continuous casting of a Fe-C-Mn thin slab (125 mm) of 1200 mm width is presented. The tundish has 60 ton capacity, and the basic properties of the steel are presented in **Table 1**.

Properties	Units	C-Mn SAE 1018 steel
Slab width	m	1.600
Slab depth	m	0.255
Casting temperature	°C	1.574
Casting speed	$m.min^{-1}$	0.810
Cooling water temperature	°C	30
Environment temperature	° C	40
Liquidus temperature	°C	1.519
End of solidification temperature	°C	1.410
Slab material		SAE 1018 steel
Emissivity		0.600
Thermal conductivity in liquid phase	$W.m^{-1}.K^{-1}$	25.400
Thermal conductivity in solid phase	$W.m^{-1}.K^{-1}$	29.700
Specific heat in BCC phase at 30–838°C	$J.kg^{-1}.K^{-1}$	783.400
Specific heat in FCC phase at 838–1416°C	$J.kg^{-1}.K^{-1}$	647.500
Specific heat in liquid phase 1416–1519°C	$J.kg^{-1}.K^{-1}$	803.200
Density of solid phase BCC 300–838°C	$kg.m^{-3}$	7.830
Density of solid phase FCC 838–1416°C	$kg.m^{-3}$	7.305
Density of liquid at 1522°C	$kg.m^{-3}$	7.034
Latent heat of solidification, ΔH	$J.kg^{-1}$	231.900

Table 1. Basic thermophysical properties of SAE 1018 (Fe-C-Mn) with simulation data.

http://dx.doi.org/10.5772/intechopen.75935

The initial step of the tundish feeling presents strong turbulence features and plays important role on the stable flowing development and security of the whole operation. **Figure 7** shows the flowing pattern (t= 3 s) for a thin slab operation while the slab extraction is off. As can be observed, the inhibitor apparatus is important to avoid splashing and protect the refractories. **Figure 8** shows the conditions where the stable flow rates are achieved with the liquid level of the tundish nearly constant. The flow pattern indicates that a complex turbulent flow is observed and the liquid flow promotes strong mixing.

In order to assure the coupled model formulation and the simultaneous solution in the parallel platform simulation, a confrontation with measured temperature profile measured in the industrial machine was performed. **Figure 9** showed a comparison of the model predictions for the serial, parallel and the pyrometer measurement at the industrial machine.

As can be observed, a close agreement with the industrial operation measurements for the temperature is reached. The measurements and calculations were compared for the stable casting operation, and the measured values were obtained using infrared pyrometer, and the plotted values are the average of five runs with intervals of 5 min.

As can be observed also, the values obtained with the serial and parallel versions are virtually the same. A complete view of the solid portion of the continuous casting domain is shown in **Figure 10** for stable flowing state. A thin skin formed in the oscillating mould region and continuous growing along the bending and cooling zones is observed. A recalescence and final cooling regions are observed. These regions are critical for the process due to the possibility of crack and defect susceptibility depending on the cooling rates and inclusions dragged and formed during the casting development [22–24].

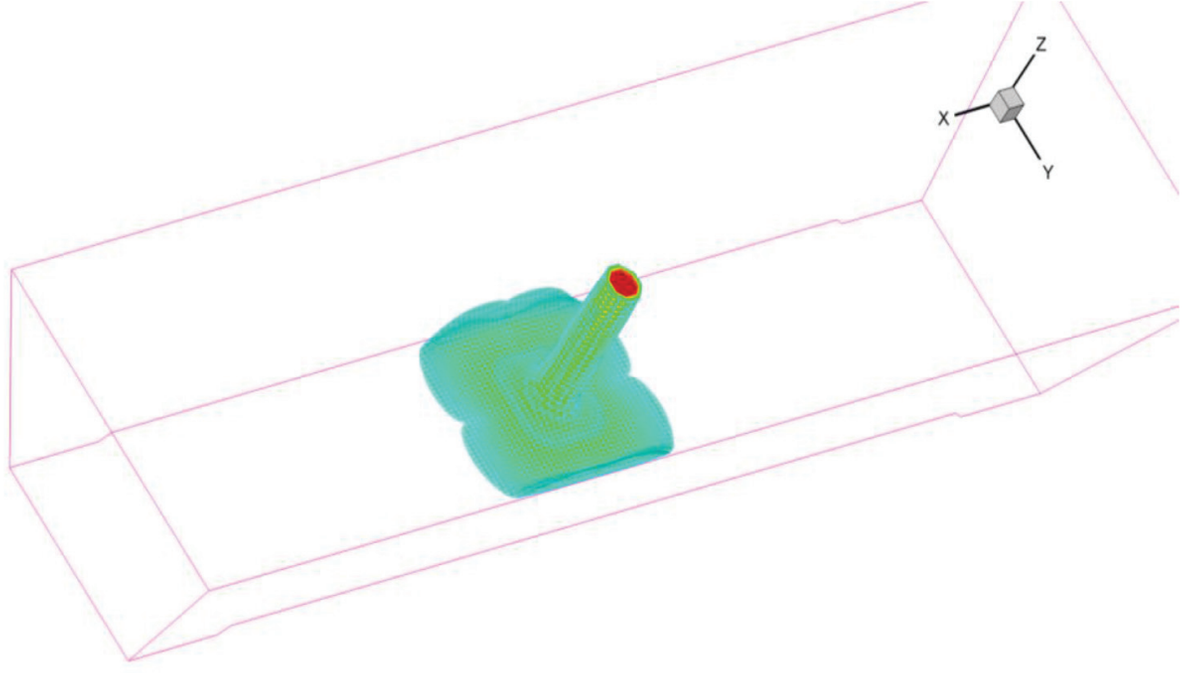

Figure 7. Fluid flow pattern during initial stage of the tundish feeling period.

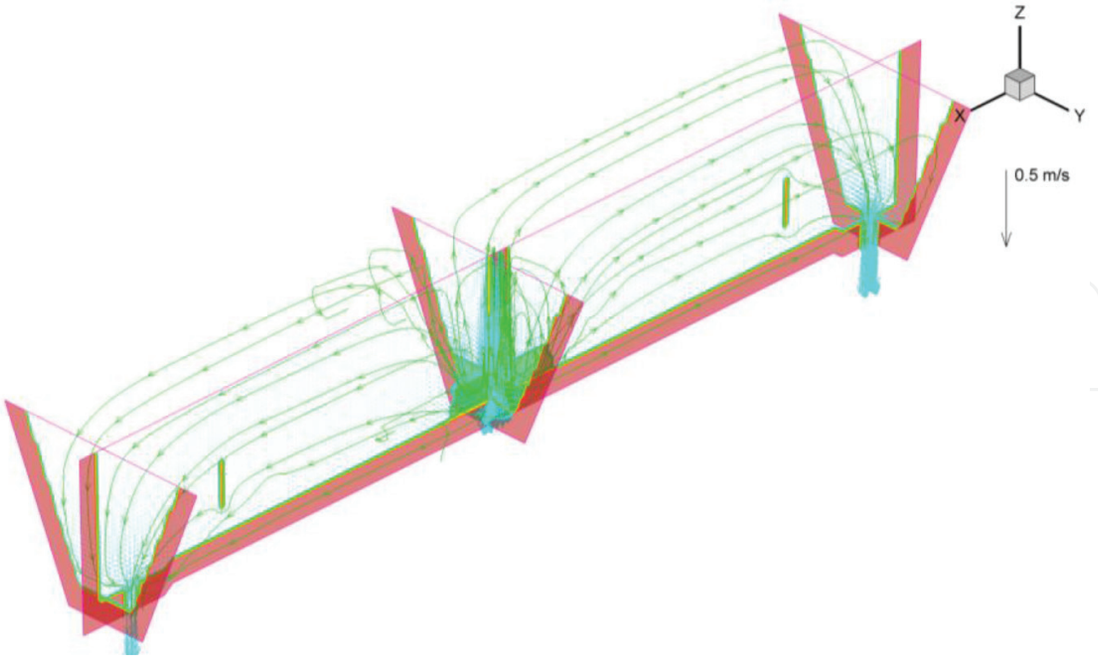

Figure 8. Fluid flow pattern obtained with the solutions of the model equations with parallel code version.

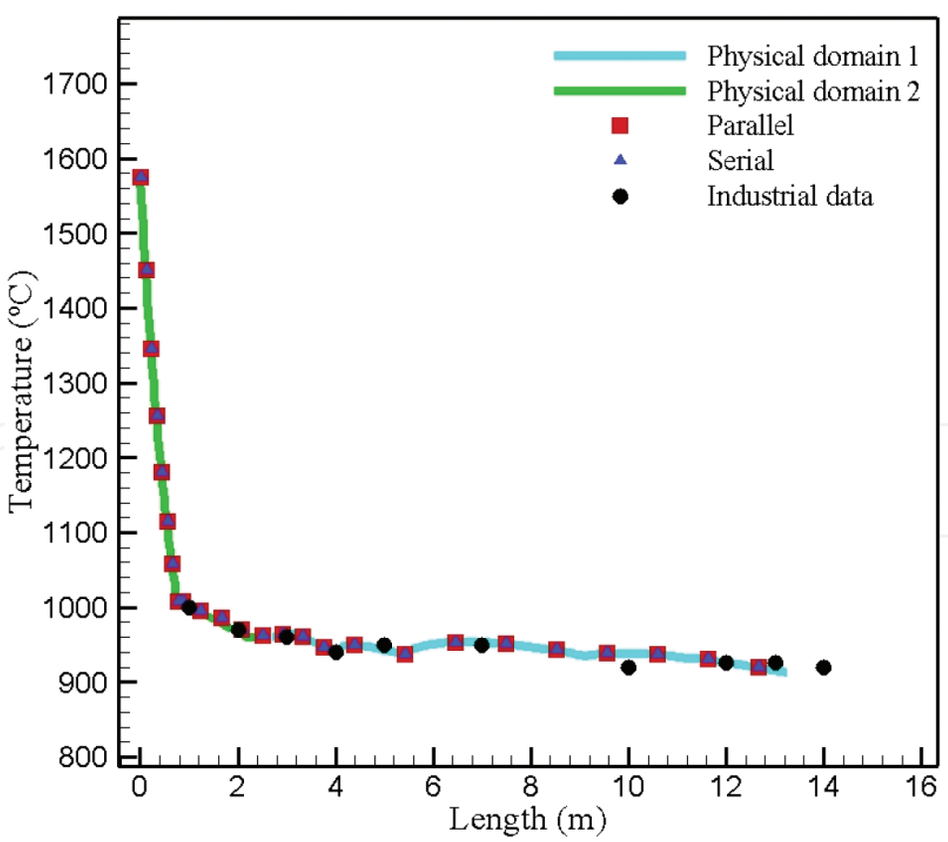

Figure 9. Model validation with industrial data acquisition along the steel slab and comparison with the solutions obtained with the serial and parallel code versions.

http://dx.doi.org/10.5772/intechopen.75935

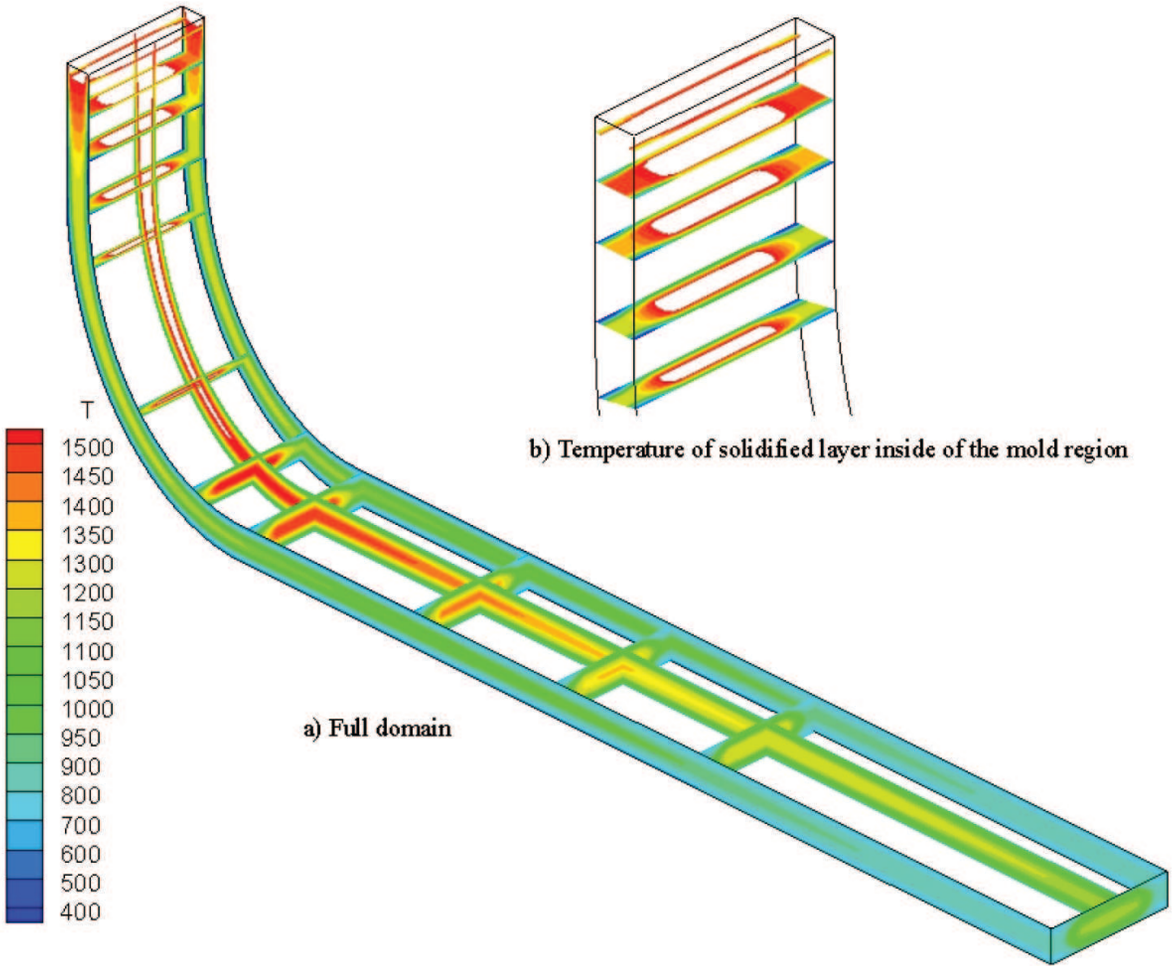

Figure 10. Full domain temperature distribution pattern and the solid skin formed during the continuous casting process of steel slab.

5. Conclusions

A unified formulation for the liquid metal flows and heat transfer within the tundish and continuous casting was presented and applied for actual industrial practices. New operational conditions for the metal flows aiming to allow the inclusion flotation and slag capture are suggested. The prediction of actual continuous casting practice is compared with industrial data. Thus, the simulation platform can be used for designing new thin slab continuous casting process, which could decrease the subsequent steps of hot rolling for thickness reduction.

Acknowledgements

Authors acknowledge financial support provided by FAPERJ (Fundação de Amparo à Pesquisa do Estado do Rio de Janeiro), CAPES (Coordenação de Aperfeiçoamento de Pessoal de Ensino superior) and CNPq (Conselho Nacional de Pesquisa)

Author details

Jose Adilson de Castro[1]*, Bruno Amaral Pereira[1], Roan Sampaio de Souza[1], Elizabeth Mendes de Oliveira[2] and Ivaldo Leão Ferreira[3]

*Address all correspondence to: joseadilsoncastro@id.uff.br

1 Federal Fluminense University (UFF/RJ), Brazil

2 Department of Metallurgical Engineering, Federal Center for Technological Education (CEFET/RJ), Angra dos Reis, Brazil

3 Department of Mechanical Engineering, Federal University of Pará (UFPA/Pa), Belém, Brazil

References

[1] Lan XK, Khodadadi JM. Fluid flow, heat transfer and solidification in mold of continuous caster during ladle change. International Journal of Heat and Mass Transfer. 2001;**44**:953-965. DOI: 10.1016/S0017-9310(00)00145-9

[2] Wang EG, He JC. Finite element numerical simulation on thermo-mechanical behavior of steel billet in continuous casting mold. Science and Technology of Advanced Materials. 2001;**2**:257-263. DOI: 200.130.19.152

[3] Luo X, Xie Q, Wang Y, Yang C. Estimation of heat transfer coefficients in continuous casting under large disturbance by Gaussian kernel particle swarm optimization method. Cuie International Journal of Heat and Mass Transfer. 2017;**111**:1087-1097. DOI: 10.1016/j.ijheatmasstransfer.2017.03.105

[4] Pardeshi R, Basak S, Singh AK, Basu B, Mahashabde V, Roy SK, Kumar S. Mathematical modeling of the Tundish of a single-strand slab caster. ISIJ International. 2004;**44**:1534-1540. DOI: 10.2355/isijinternational.44.1534

[5] Ha MY, Lee HG, Seong SH. Numerical simulation of three-dimensional flow, heat transfer and solidification of steel in continuous casting mold with electromagnetic brake. Journal of Materials Processing Technology. 2003;**133**:322-339. DOI: 10.1016/S0924-0136(02)01009-9

[6] Janik M, Dyja H. Modelling of three-dimensional temperature field inside the mould during continuous casting of steel. Journal of Materials Processing Technology. 2004;**157**: 177-182. DOI: 10.1016/j.jmatprotec.2004.09.026

[7] Peng X, Zhou J, Qin Y. Improvement of temperature distribution in continuous casting moulds through the rearrangement of the cooling water slots. Journal of Materials Processing Technology. 2005;**167**:508-514. DOI: 10.1016/j.jmatprotec.2005.05.023

[8] Choudhary SK, Mazumdar D, Ghosh A. Mathematical modeling of heat transfer phenomena in continuous casting of steel. ISIJ International. 1993;**33**:764-774. DOI: 0915-1559

[9] Zhou L, Wang W, Xu C, Chen Z. An investigation of the mold-flux performance for the casting of Cr12MoV steel using a mold simulator technique. Metallurgical and Materials Transactions. 2017;**48**:2017-2026. DOI: 10.1007/s11663-017-0990-0

[10] Maurya A, Jha - Pradeep K. Influence of electromagnetic stirrer position on fluid flow and solidification in continuous casting mold. Applied Mathematical Modelling. 2017;**48**:736-748. DOI: 10.1016/j.apm.2017.02.029

[11] Spinelli JE, Tosetti JP, Santos CA, Spim JA, Garcia A. Microestruture and solidification thermal parameters in thin strip continuous casting of stainless steel. Journal of Materials Processing Technology. 2004;**150**:255-262. DOI: 10.1016/j.jmatprotec.2004.02.040

[12] Thomas BG, Mika LJ, Najjar FM. Simulation of fluid flow inside a continuous slab-casting machine. Metallurgical Transactions B. 1990;**21B**:387-400. DOI: 0360-2141

[13] Chan YW. Finite element simulation of heat flow in continuous casting. Advanced Engineering Software. 1989;**11**:128-135. DOI: 10.1016/0141-1195(89)90042-9

[14] Brian GT, Fady MN. Finite element modeling of turbulent fluid flow and heat transfer in continuous casting. Applied Mathematical Modelling. 1991;**15**:226-243. DOI: 10.1016/0307-904X(91)90001-6

[15] Sheng-Long J, Zheng Z, Liu M. A multi-stage dynamic soft scheduling algorithm for the uncertain steelmaking-continuous casting scheduling problem. Applied Soft Computing. 2017;**60**:722-736. DOI: 10.1016/j.asoc.2017.07.016

[16] Husepe AE, Cardona A, Fachinotti V. Thermomechanical model of continuous casting process. Computer Methods in Applied Mechanics Engineering. 2000;**182**:439-455. DOI: 10.2478/v10172-012-0034-3

[17] Vasta VN, Hammond DP. Viscous flow computations for complex geometries on parallel computers. Advances in Engineering Software. 1998;**29**:337-343. DOI: 10.1016/S0965-9978(97)00076-8

[18] Sikora J, Ramakrishnan S, Leblanc L. Conversion of a single process CFD code to distributed and massively parallel processing. Advanced Engineering Software. 1998;**29**:331-336. DOI: 10.1016/S0965-9978(98)00007-6

[19] Lepper J, Schnell U, Hein KRG. Parallelization of a simulation code for reactive flows on the intel paragon. Computers & Mathematics with Applications. 1998;**35**:101-109. DOI: 10.1016/S0898-1221(98)00037-6

[20] Nesterov O. A simple parallelization technique with MPI for ocean circulation models. Journal of Parallel and Distributed Computing. 2010;**70**:35-44. DOI: 10.1016/j.jpdc.2009.09.005

[21] Moreira LP, Castro JA. Modeling the hot rolling process using a finite volume approach. Transactions on Engineering Sciences. 2008;**59**:419-430

[22] Zienkiewicz OC. Flow of solids during forming and extrusion: Some aspects of numerical solutions. International Journal of Solids and Structures. 1978;**14**:15-38. DOI: 10.1016/0020-7683(78)90062-8

[23] Holman JP. Heat Transfer. 7th ed. New York, NY: Mc Graw-Hill Book Company; 1990

[24] Ferreira IL, Voller VR, Nestler B, Garcia A. Two-dimensional numerical model for the analysis of macrosegregation during solidification. Computational Materials Science. 2009;**46**:358-366. DOI: 10.1016/j.commatsci.2009.03.020

[25] Melaaen MC. Calculation of fluid flows with staggered and nonstaggered curvilinear nonorthogonal grids—The theory. Numerical Heat Transfer-Part B. 1992;**21**:1-19

[26] Patankar VS. Numerical Heat and Fluid Flow. 2nd ed. Washington, DC: Hemisphere Publishing Corp; 1980. 197 p. DOI: 007084740-5